A Robust Hybrid Control for Autonomous Flying Robots in an Uncertain and Disturbed Environment

Yunes Sh. ALQUDSI*,[1], Ayman H. KASSEM[1], Gamal M. El-BAYOUMI[1]

*Corresponding author
[1]Aerospace Engineering, Cairo University,
Giza, 12613, Egypt,
yunes.sharaf@pg.cu.edu.eg*

DOI: 10.13111/2066-8201.2021.13.2.17

Received: 17 April 2021 / Accepted: 11 May 2021 / Published: June 2021

Abstract: *With the aim of efficiently achieving complex trajectory tracking missions in the presence of model uncertainties and exogenous disturbances, this paper proposes a robust hybrid control for the orientation and position of flying robots by adopting insights from sliding mode, geometric tracking, and nonlinear feedback control strategies. Various retrofits are implemented to the composite control scheme in order to tackle the system uncertainties, eliminate the chattering effects, and enhance the trajectory tracking performance. The convergence and stability analysis demonstrated the asymptotic stability of the proposed control algorithm. To reveal the promising performance of the developed control schemes, a qualitative comparative analysis of different proposed control approaches is performed. The comparative analysis examines highly maneuverable trajectories for various tracking scenarios in the presence of uncertain disturbances. The simulation results demonstrated the versatility, robustness, and convergence of the developed control laws that allow autonomous flying robots to effectively perform agile maneuvers.*

Key Words: *Robust Control, Sliding Mode Control, Trajectory Tracking, Nonlinear Control, Chattering Effect; Quadrotor Robot*

1. INTRODUCTION

Due to their versatility, agility, and cost advantages the quadrotor aerial robots considered as one of the most attractive (UAVs, MAVs) platforms in academic and industrial researches. Unlike the fixed-wing UAVs and conventional helicopters, the hover capability combined with fabrication simplicity have given preference to quadrotors in commercial, agricultural, and civilian applications and even in military applications. Numerous researches concerning the applications of quadcopter UAVs have been published. For instance, in navigation and localization [1], [2], flying manipulation [3], object transportation [4], and in surveillance and monitoring activities [5]. In view of the fact that quadrotor robot is an underactuated, dynamically coupled, and highly nonlinear system, the design of its control system has opened up a wide area of research and attracted many developers and researchers with the aim of achieving an accurate trajectory tracking performance, asymptotic stability and convergence for the UAVs control systems. Recently, several control strategies for quadrotor robots have been developed to meet the requirements of the UAVs applications in various areas of interest. For the purpose of relatively low maneuverability and velocities, many linear control algorithms have been implemented such as the PID control family [6], linear quadratic-

regulator (LQR) control [7]. To overcome the limitations and drawbacks of linear controllers, the researchers have been proposed several advanced nonlinear control schemes for highly maneuverable drones including linear parameter varying (LPV) control [8], fuzzy and neural network controls [9], [10], adaptive control [11], combined and geometric tracking control [12]–[14], backstepping control [15], [16], model predictive control [17], and sliding mode control [18]–[22]. The valuable work of [11], proposed the sliding mode-based control that assumed small roll and pitch angles to arrive at a linearized dynamical model of the quadrotor. They used a continuous adaptive dynamic vector to eliminate the chattering effect to achieve the asymptotic stability and enhance the tracking performance. Based on the finite-time stability theory and geometric control, the study of [14] proposed a discrete-time control scheme to gain better implementation in the onboard computers and arrive at an improved steady-state performance. The effect of the time-varying measurement delay and uncertain disturbances on quadrotor systems have been investigated in [15], to provide robust tracking performance and smooth input acquisition. The quadrotor input constraints and external disturbances are considered in [16]. They suggested a prescribed performance backstepping dynamic surface control (DSC) scheme to improve the stability of the quadrotor and simplify the controller design process. The simulation results demonstrated an acceptable tracking error and a satisfying steady-state performance. In [18], the authors proposed a controller split into two parts; a sliding mode-based controller to control the quadrotor attitude and a linear PD controller for the position and altitude control. For the position and altitude controllers, they assumed small yaw, pitch, and roll angles. Hence, based on the imposed assumptions, the simulation results showed satisfactory stability and performance. Reference [19], proposed a control approach based on the sliding mode observer with finite-time process, hybridized PID controller, and continuous sliding-mode control. The two main aims of their work were to estimate the system state vector based on the measured output states and to track the desired time-varying trajectory regardless of the influence of uncertainties or external disturbances. The authors of [23], developed a disturbance observed DO-based SMC. In their study, the desired control performance is achieved by transferring the system state from an unstable state to a steady state. The simulation results of their work showed a good convergence for altitude and attitude control. Authors of [24], utilized the feedback linearization in addition to PID and LQR controllers so as to design a position-tracking model and optimize the control algorithm by determining a suitable cost function for LQR and hence optimize the tracking performance. Among the various nonlinear control algorithms, SMC and its different versions have gained remarkable significance due to their robustness, time optimality, and ability to overcome uncertainties and disturbances [20]. Hence, in this study, we've decided to exploit the advantages of the SMC in a new synthesis control to arrive at a promising tracking performance for the UAVs.

1.1 Motivation and Contribution of the Paper

This study mainly focuses on the trajectory tracking control performance of aerial robots, taking into account the orientation and position controls, complete nonlinear dynamics, model uncertainties, and disturbance sources that may affect the system's overall performance. The novelty of this study is represented by the new composite control scheme that integrates certain nonlinear control algorithms with some retrofits to arrive at better stability and improved steady-state performance. More specifically, novel robust hybrid control laws based on the SMC, geometric tracking control (GTC), and nonlinear feedback control (NFC) are derived including adjustments to tackle the drawbacks associated with each component separately. For instance, we consider modifying the conventional SMC to eliminate the chattering effect and

accurately achieve complex tracking missions by using adjustable saturation function and along with the exponential reaching law (ERL). The rest of this paper is organized as follows: section 2 briefly mentions the main features and configurations of the quadrotor aerial robots. Then, a concise description of the nonlinear dynamic model of quadrotor UAVs is provided in the third section. The formulation and considerations of the control problem in addition to the proposed robust hybrid control schemes are derived and discussed in section 4. In the convergence and stability analysis section, Lyapunov's stability approach is used to examine and prove the asymptotic stability of the proposed controllers. The considerations and tuning procedure of the controllable parameters are then mentioned. Subsequent qualitative comparative analysis (QCA) and simulation results are presented to exhibit the robustness, effectiveness, asymptotic stability, superiority, and applicability of the proposed control schemes.

2. QUADROTOR FEATURES AND CHARACTERISTICS

The configuration and coordinate system of quadrotor UAVs are shown in Fig. 1, in which its four rotors are directed upward in order to provide the necessary lifting force and moments, namely the roll, pitch, and yaw moment about x, y and z , respectively.

The quadrotor basic motions in the 3D space are achieved by varying the speed of its four motors. The six translational and rotational degrees of freedom (DOF) are controlled via four input DOFs, namely the thrust magnitude of four rotors, to arrive at asymptotic trajectory tracking of four desired outputs, that is the three components of the robot c.g. position vector and its heading angle.

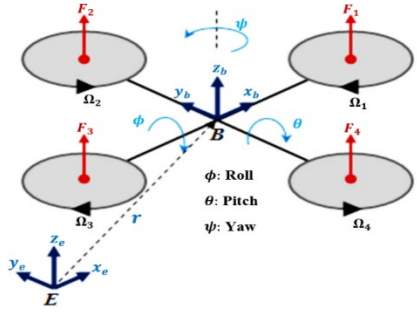

Fig. 1 Quadrotor Model and Coordinate System

The rotation direction of rotors (1,3) in Fig. 1, is the opposite of that of rotors (2,4) to prevent unwanted yaw motion. For upward-downward motions along the z-axis, the speed of all motors increases or decreases simultaneously. The two well-known configurations of quadrotor UAVs are plus (+) and cross (×) configurations. In the quadrotor with plus-configuration, the motion along the x-axis is carried out by tilting the robot i.e. by making the speeds of rotors (1,3) different. The same way is true for the motion along the y-axis through rotors (2,4). Regarding the yaw motion about the z-axis, in order to rotate the quadrotor counterclockwise, we increase the speed of clockwise rotors i.e. rotors (1,3).

It is worth mentioning that, for plus and cross configurations as shown in Fig. 2, the yaw mode is obtained with the same scenario mentioned above. On the other hand, the roll and pitch motions in the plus-config required only two rotors to achieve the motion, however, in the cross-config, the four rotors rotate in a certain way to generate the motion. For instance, to move the quadrotor robot of cross-config along the x-axis, we need to increase $(\Omega_{NW}, \Omega_{SW})$ compared to $(\Omega_{NE}, \Omega_{SE})$.

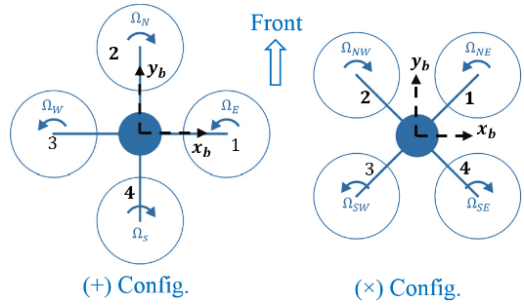

Fig. 2 Quadrotor Plus and Cross Configurations

In cross-config, as the rotation direction of $(\Omega_{NW}, \Omega_{SW})$ is opposite during the motion along the x-axis, the resultant yaw torque is canceled out. Thus, pitch and roll control don't generate a net yaw moment in contrast with plus-config. Moreover, for the same desired motion, the momentum introduced by the cross-config is greater resulting in higher maneuverability as the roll and pitch modes require the four rotors to simultaneously change their speeds to achieve the motion. However, the attitude control for both plus and cross configurations is essentially analogous [21].

3. NONLINEAR DYNAMIC MODEL

As depicted in Fig. 1, the quadrotor dynamics are derived in both inertial, E and body, B coordinate systems, so that, the body frame is attached to the center of mass (c.g.) of the quadrotor robot. The position vector of the robot c.g. with respect to the fixed world frame is denoted by $r = [x, y, z]^T$. The considerable forces affecting the robot are the gravity force in the ($-z_e$) direction, and the thrust forces of all rotors along (z_b) axis. Hence, using Newton's approach, the linear acceleration of the robot c.g. is governed by the following vector equation,

$$m\,\ddot{r} = -m\,g\,\hat{z}_e + u_1\,R\,\hat{z}_b \tag{1}$$

where, m is the quadrotor mass, g is referred to as the acceleration of gravity, $u_1$is the summation of thrust forces of four rotors, and $\hat{z}_e$, $\hat{z}_b$ are the 3rd unit vector of the inertial and body frames respectively. In this study, we adopt the (Z-X-Y) convention for Euler angles to transform coordinates from body to inertial frame. Thus, the rotation matrix is given by,

$$R = \begin{bmatrix} c_\psi\,c_\theta - s_\phi\,s_\psi\,s_\theta & -c_\phi\,s_\psi & c_\psi\,s_\theta + c_\theta\,s_\phi\,s_\psi \\ c_\theta s_\psi + c_\psi s_\phi s_\theta & c_\phi c_\psi & s_\psi s_\theta - c_\psi c_\theta s_\phi \\ -c_\phi s_\theta & s_\phi & c_\phi c_\theta \end{bmatrix} \tag{2}$$

where, $c_{(*)}$ and $s_{(*)}$ denote $\cos(*)$ and $\sin(*)$, respectively and ϕ, θ, and ψ are the roll, pitch, and yaw angles, respectively. According to our rotation convention, the angular velocity components of the quadrotor in the body frame (p, q, r) are related to the derivatives of the roll, pitch, and yaw angles according to,

$$\begin{bmatrix} p \\ q \\ r \end{bmatrix} = \begin{bmatrix} c_\theta & 0 & -c_\phi s_\theta \\ 0 & 1 & s_\phi \\ s_\theta & 0 & c_\phi c_\theta \end{bmatrix} \begin{bmatrix} \dot{\phi} \\ \dot{\theta} \\ \dot{\psi} \end{bmatrix} \tag{3}$$

The vector equation governing the quadrotor angular acceleration is obtained using the Euler approach as follows,

$$I\,\dot{\omega} = U_2 - \omega \times I\,\omega \tag{4}$$

where $\omega = [p \quad q \quad r]^T$, I is a matrix representing the robot's moment of inertia, and U_2 is the torque vector which is defined based on the robot configuration as follows,

$$U_2 = \begin{bmatrix} \ell(\mathrm{c} * (\mathrm{F}_1 - \mathrm{F}_3) + \mathrm{F}_2 - \mathrm{F}_4) \\ \ell(\mathrm{c} * (\mathrm{F}_2 - \mathrm{F}_4) + \mathrm{F}_3 - \mathrm{F}_1) \\ \tau_1 - \tau_2 + \tau_3 - \tau_4 \end{bmatrix}, \tag{5}$$

Where c equals zero and one, respectively, for quadrotor with Plus and Cross configurations. ℓ is the moment arm representing the distance from the rotor axis of rotation to the center of the aerial robot. F_i and τ_i are the thrust force and torque, respectively, generated by rotor_i , $i \in \{1,2,3,4\}$. Each robot has an angular velocity, Ω_i produces thrust force, F_i and torque, τ_i according to:

$$\mathrm{F}_i = \mathrm{k}_f\,\Omega_i^2 \quad , \quad \tau_i = \mathrm{k}_m\,\Omega_i^2 \tag{6}$$

where, Ω_i is the angular velocity of rotor_i. The desired control action u_{des} which includes the net force of all rotors and the three torque components namely, u_1 and U_2 is related to the desired rotor speeds vector according to the robot configuration.

$$u_{\mathrm{des}} = \begin{bmatrix} \mathrm{k}_f & \mathrm{k}_f & \mathrm{k}_f & \mathrm{k}_f \\ c\,\mathrm{k}_f\ell & \mathrm{k}_f\ell & -\mathrm{c}\,\mathrm{k}_f\ell & -\mathrm{k}_f\ell \\ -\mathrm{k}_f\ell & c\,\mathrm{k}_f\ell & \mathrm{k}_f\ell & -\mathrm{c}\,\mathrm{k}_f\ell \\ \mathrm{k}_m & -\mathrm{k}_m & \mathrm{k}_m & -\mathrm{k}_m \end{bmatrix} \begin{bmatrix} \Omega^2{}_{des,1} \\ \Omega^2{}_{des,2} \\ \Omega^2{}_{des,3} \\ \Omega^2{}_{des,4} \end{bmatrix} \tag{7}$$

where, $\mathrm{k}_f, \mathrm{k}_m$ are the thrust and drag coefficients, respectively. According to the nonlinear quadrotor model, the robot system has twelve states and four inputs. The system state includes the position and linear velocity of the quadrotor c.g., in addition to the components of orientation and angular velocities. The robot orientation is locally parametrized by Euler angles.

$$X = [x\,, y\,, z\,, \dot{x}\,, \dot{y}\,, \dot{z}\,, \phi\,, \theta\,, \psi\,, p\,, q, r]^T, \quad \text{Inputs} = [\Omega_1\,,\ \Omega_2\,,\ \Omega_3\,,\ \Omega_4]^T$$

For the quadrotor, in order to follow the desired trajectory, the four inputs to the controller are the $x^{des}, y^{des}, z^{des}$, and the heading angle ψ^{des}. In the robot mathematical model, we neglected the effect of motor dynamics and the forces with a minor influence such as the aerodynamics "induced drag-force". Because the motor dynamics are relatively fast compared to that of the quadrotor, it's usually assumed to be instantaneously achieved. Since the induced drag is very small, its effect can be included in the disturbance term [25]. However, in this paper, the effect of motor dynamics and neglected forces will be taken into account during the controller design procedure.

4. SYNTHESIS AND ANALYSIS OF THE ROBUST HYBRID CONTROLLER

This section concentrates on the robust control strategy, namely, a hybrid SMC, GTC, and NFC to exploit its capability of asymptotically achieve the demanded performance regardless of system uncertainties or external disturbance, given that, the upper and lower bounds or at least the upper bound of the uncertain disturbances are known. The main preliminaries and notions about the conventional SMC are provided in the Appendix.

To start developing the proposed control schemes, at first, some modifications will be conducted to the classical SMC. More precisely, two additional terms will be added to Eq. (33) and the signum function will be replaced by a time-variant saturation function as follows;

$$\delta(t) = -\eta\, S\, sat\,(S/\varphi) - K\, S^2 + \dot{\varphi}\, S\, sat\,(S/\varphi) \tag{8}$$

Such that,

$$\dot{S} \leq (\dot{\varphi} - \eta)\ sat\,(S/\varphi) - K\, S \tag{9}$$

The time-variant saturation function, $sat\big(S/\varphi(t)\big)$ is determined according to,

$$sat(S/\varphi) = \begin{cases} 1 & S > \varphi \\ S/\varphi & -\varphi \leq S \leq \varphi \\ -1 & S < -\varphi \end{cases} \tag{10}$$

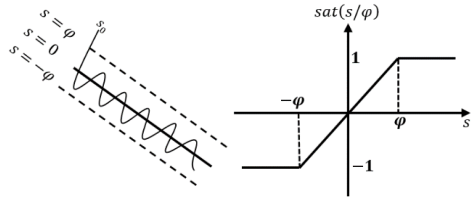

Fig. 3 The Saturation function schematic diagram

The parameter $K > 0$, comes from ERL to improve the tracking performance [26], [27], while the saturation function $sat\ (*)$ is used instead of signum function $sign\ (*)$ to resolve the chattering phenomenon since it provides a smooth transition between (1) and (-1). Furthermore, to gain the advantage of signum function in that the steady-state error almost equal to zero, the transition interval of the saturation function $sat\ (S/\varphi)$ is chosen to be a controllable parameter represented by φ such that, φ smoothly tends to zero hence, the saturation function switches to signum function. Since we have relaxed the sliding mode condition by using time-variant saturation function, then the time-varying parameter, $\dot{\varphi}$ should be added to ensure that when S enters the transition interval, $[-\varphi, \varphi]$ it will always remain there, which mean if φ shrinks then S should shrink at the same rate or faster i.e. $\dot{\varphi} \geq S^2$ [28]. The value of φ depends on the system dynamics and the tunable parameters (η, C, K) therefore, we arrive at better steady state error than that of $sat\ (S)$. In another words, φ plays a role in the trade-off between steady state error and chattering effect.

4.1 Robust Hybrid Control Design

In this section, the modified SMC with ERL will be integrated with GTC and NFC. In order to consider the uncertain disturbances, uncertainty terms will be added to the quadrotor equations of motion derived in Eq. (1) and Eq. (4), to arrive at,

$$\ddot{\mathrm{r}} = -g\, \hat{z}_e + 1/m\ u_1\, R\, \hat{z}_b + \Delta_1(t) \tag{11}$$

$$\dot{\omega} = I^{-1}\,(-\omega \times I\,\omega) + I^{-1}\, U_2 + \Delta_2(t) \tag{12}$$

where, $\Delta_1(t)$ and $\Delta_2(t)$ are vectors that represent the virtual uncertainties and disturbances in the robot system such that, $\Delta_1(t)$ includes the uncertainties in x, y, and z, while the attitude uncertainties are included in $\Delta_2(t)$ where,

$$\Delta_{1L} \leq \Delta_1(t) \leq \Delta_{1U}\ , \qquad \Delta_{2L} \leq \Delta_2(t) \leq \Delta_{2U}$$

4.1.1 Position Control Design

According to the problem formulation and the quadrotor's governing equations, Eq. (11) and Eq. (12),

$$f_{3\times1} = -g\,\hat{z}_e\ ,\ \ g_{3\times1} = \frac{1}{m} R\,\hat{z}_b\ ,\qquad e_{3\times1}(t) = r_{des}(t) - r(t)$$

Let, $\mathcal{H}_{3\times1} = f + \Delta_1(t)$. The sliding surface vector-equation is defined as,

$$S = \dot{e} + C_p\, e, \tag{13}$$

By taking the derivative of the sliding surface in Eq. (13), we arrive at,

$$\dot{S} = \ddot{r}_{des} - \ddot{r} + C_p\,\dot{e} = \ddot{r}_{des} - \mathcal{H} - g\,u_1 + C_p\,\dot{e} \tag{14}$$

We defined u_1 as a summation of two terms $\hat{u}_1$ and u_{1_uncer} multiplied by g^{-1} such that,

$$\hat{u}_1 = \ddot{r}_{des} + C_p\,\dot{e} - \widehat{\mathcal{H}}, \tag{15}$$

$$u_{1_{uncer}} = (\mathcal{F} + \eta_P)\, sat(S/\varphi_P) + K_P\, S\,, \tag{16}$$

where, $\widehat{\mathcal{H}}$ is the best possible estimation of $\mathcal{H}$. The lower limit of the difference between $\mathcal{H}$ and its estimation is represented by $\mathcal{F}$ such that, $\mathcal{F} \geq \left|\mathcal{H} - \widehat{\mathcal{H}}\right|$. We choose $\widehat{\mathcal{H}}$ to be the average of $\mathcal{H}$,

$$\widehat{\mathcal{H}} = -g\,\hat{z}_e + 0.5\,(\Delta_{1U} + \Delta_{1L})\quad ,\qquad \mathcal{F} = 0.5\,(\Delta_{1U} - \Delta_{1L}) \tag{17}$$

Hence, the effect of φ_P will be considered in $u_{1_{\text{uncer}}}$ so that, the sliding condition is always met [28]. The values of $u_{1_{\text{uncer}}}$ and φ_p are determined according to,

$$u_{1_{\text{uncer}}} = (\mathcal{F} + \eta_P - \dot{\varphi}_P)\, sat\big(S/\varphi_p\big) + K_P\, S\,, \tag{18}$$

$$\dot{\varphi}_P = (K_P - C_P)\varphi_P + (\mathcal{F} + \eta_P) \tag{19}$$

After putting the two terms of u_1 together we arrive at,

$$R\,\hat{z}_b\ u_1 = m\big(\ddot{r}_{des} + C_p\,\dot{e} + g\,\hat{z}_e - \gamma_{2P} + (\eta_P - \dot{\varphi}_P + \gamma_{1P})\, sat(S/\varphi_P) + K_P\, S\big) \tag{20}$$

where, $\gamma_{1P} = 0.5\,(\Delta_{1U} - \Delta_{1L})$, $\gamma_{2P} = 0.5\,(\Delta_{1U} + \Delta_{1L})$.

Obviously, u_1 which represents the resultant thrust of the four rotors, is a scalar quantity applied only along the actual body-frame z-axis i.e. along $\hat{z}_b$ direction. From the inertial-axes perspective, u_1 is along the vector,

$$\hat{b}_{3w} = R\,\hat{z}_b \tag{21}$$

Let the 3D vector of the r.h.s. of Eq. (20) be equal to h_{vec},

$$h_{vec} = m\big(\ddot{r}_{des} + C_p\,\dot{e} + g\,\hat{z}_e + K_P\, S - \gamma_{2P} + (\eta_P - \dot{\varphi}_P + \gamma_{1P})\, sat(S/\varphi_P)\ \big) \tag{22}$$

Since the resultant thrust, u_1 is acting on the quadrotor along $\hat{b}_{3w}$ therefore, to determine u_1 we will project h_{vec} onto $\hat{b}_{3w}$ [13]. Therefore, the proposed robust hybrid position-control law is determined according to,

$$u_1 = m(\,\ddot{r}_{des} + C_p\,\dot{e} + g\,\hat{z}_e + K_P\, S - \gamma_{2P} + sat(S/\varphi_P)\,(\eta_P - \dot{\varphi}_P + \gamma_{1P})\,).R\,\hat{z}_b \tag{23}$$

4.1.2 Attitude Control Design

By following the same procedure conducted in the position control design with,

$$f_{3\times1} = I^{-1}(-\omega \times I\,\omega)\ , \quad g_{3\times1} = I^{-1}, \quad e_{3\times1}(t) = e_R(R^{des}, R), \quad \dot{e}_{3\times1}(t) = e_\omega(\omega^{des}, \omega),$$
$$\ddot{e}_{3\times1}(t) = \dot{\omega}(t) - \dot{\omega}^{des}(t)$$

then, the proposed vector control law of the attitude control, $U_2 \in \mathbb{R}^3$ is determined as follows,

$$U_2 = \omega \times I\,\omega + I\left(\dot{\omega}^{des} + C_R\,\dot{e} + K_R\,S - \gamma_{2R} + (\eta_R - \dot{\varphi}_R + \gamma_{1R})\,sat(S/\varphi_R)\right) \quad (24)$$

where, $\gamma_{1R} = 0.5\,(\Delta_{2U} - \Delta_{2L}), \gamma_{2R} = 0.5\,(\Delta_{2U} + \Delta_{2L})$. At this point, an essential aspect to be considered is the way in which the rotation error, $e_R(t)$ is calculated. One method to do so is by first find a way to determine what's so-called the desired rotation matrix, R^{des}, then find a way to extract a metric representation for the error between the actual and desired rotation matrices. In this context, as the direction of h_{vec} is, $\hat{h}_{vec} = h_{vec}/\|h_{vec}\|$, and generally, h_{vec} is not perfectly aligned with $\hat{b}_{3w}$, and we want the direction of h_{vec} to be always aligned with $\hat{b}_{3w}$. In another meaning, to ensure that $\hat{b}_3$ is aligned with $\hat{h}_{vec}$, then we rotate the quadrotor by R^{des} so that $\hat{z}_\mathrm{b}$ points to the direction of $\hat{h}_{vec}$,

$$\hat{h}_{vec} = R^{des}\,\hat{z}_\mathrm{b} \quad (25)$$

By solving the vector Eq. (25), given that the heading angle ψ^{des} is known, we can determine φ^{des} & θ^{des} and thus determine R^{des}. The next step is to determine, $e_R(t)$. Unfortunately, we can't simply subtract R from R^{des} to get e_R, since the result is not an orthogonal matrix and thus not a rotation matrix. However, we can think of the rotation error as if we were looking for the magnitude of rotation required to go from the current to the desired orientation, namely, transform R into R^{des}. Thus, the required rotation is,

$$\Delta R = R^T R^{des}, \quad (26)$$

So that, if you multiply R by ΔR you will get R^{des}. By using Rodrigues formula to transform the rotation matrix obtained in Eq. (26) into a vector representing the axis of rotation, we arrive at a vector that will be considered as a metric for $e_R(t)$. It is worth mentioning that, the proposed control law required full state measurement or estimation, and a smooth differentiable desired trajectory, at least up to the 2nd derivative. The derived control scheme obtained in Eq. (23) and Eq. (24), illustrated that the chattering dilemma apparently depends on $(\eta - \dot{\varphi} + \gamma_1(\Delta))$, and according to Eq. (19), $\dot{\varphi}$ is function of (K_P, C_P, Δ, η), which mean that, apart from the controller variables (η, C, K), the percentage of parameter uncertainties in addition to the sources of disturbances have a great impact on the chattering phenomenon.

4.2 Convergence and Stability Analysis

To verify the stability and convergence of our proposed control algorithms, Lyapunov's stability approach will be adopted. The procedure is identical either for the position or orientation controllers, here the position control law will be considered.

If we select Lyapunov function as, $V = 1/2\,S^2$, then according to Lyapunov, to guarantee asymptotical stability it's required that $\dot{V} < 0$, or $S\,\dot{S} < 0$. For position control low,

$$\dot{V} = S\left[\ddot{r}_{des} - \ddot{r} + C_p\,\dot{e}\right] \quad (27)$$

By substituting about $\ddot{r}$ from (11) and then substitute about $(R\,\hat{z}_b\ u_1)$ from (20), we arrive at,

$$\dot{V} = S\left[(\dot{\varphi}_P - \eta_P)\,sat(S/\varphi_P) - K_P\,S + D - \Delta_1(t)\right] \quad (28)$$

where, $D = \gamma_{2P} - \gamma_{1P}\,sat(S/\varphi_P)$. The first two terms of Eq. (28) corresponding to Eq. (9), and since $D - \Delta_1(t)$ is negative for $S > \varphi_P$ and positive for $S < -\varphi_P$ hence, Eq. (28) satisfying the asymptotical stability; starting from any initial condition, S will enter the

transition set and stay there. Inside the interval and based on Eq. (19) $\dot{S}$ will follow a first order dynamics and exponentially reaching to zero according to,

$$\dot{S} = -C_P\, S + \gamma_{2P} - \Delta_1(t) \tag{29}$$

4.3 Tuning the Controllable Parameters

Several aspects should be considered during the controllable parameters tuning process of the proposed control approaches. For instance, the actuators' physical limits, unmodeled dynamics, and key performance indicators (KPIs) such as steady state-error, percent overshoot, and time response indicators. All the tuning parameters, $C,\ \eta,$ and K for the position and attitude control are positive scalar values. The parameter φ is determined according to Eq. (19) with an initial value $\varphi_0 \geq S_0$ to ensure that S is within the interval, $[-\varphi, \varphi]$ where Eq. (19) is applicable [28]. The parameter η affects the reaching time to the sliding surface and thus the chattering phenomenon. Choosing η is a trade-off as if η increases, the reaching time decreases but the chattering increases and therefore the tracking error and vice versa. For actuators that can endure the chattering effect for example those using the pulse-width modulation (PWM), it is desirable to increase η so that faster reaching to the sliding surface is achieved from any initial value of S. Selecting C value is more obvious, the greater the value of C, the better the tracking error and the faster the performance, however, the control action is proportional to C, then the upper limit of C is restricted to the saturation point of the actuator. Furthermore, the unmodeled dynamics such as motors dynamics should be considered such that C has to be dominant, usually slower by a factor (3 to 5) [28]. Likewise, the parameter K has the same influence as C moreover, it introduces a term in the control law that is proportional to the error and its derivatives, which result in faster forcing the state to reach the sliding manifold when S is large [27]. Our hybrid control scheme is a synthesis of NFC, GTC, and SMC which includes ERL and saturation function $sat(S/\varphi)$, where $\varphi(t)$ is a controllable time-varying parameter. So that, asymptotic stability is achieved, improved tracking performance is reached, and the chattering effect is almost eliminated.

5. QUALITATIVE COMPARATIVE ANALYSIS AND SIMULATION RESULTS

The derived robust hybrid control algorithms presented in the previous section are simulated using MATLAB to observe and evaluate the performance of the proposed robust controller. Quadrotor robot nominal parameters, as well as the initial conditions, are presented in Table 1. The simulation is performed under two different situations, (i) without disturbance and/or parameter uncertainties, and (ii) with disturbance and/or parameter uncertainties. The comparative analysis study is carried out for four major control schemes:

1. The PID controller with a quadrotor nonlinear model.
2. The nonlinear GTC proposed in [13].
3. The conventional SMC with ERL.
4. The robust hybrid control law proposed in this paper.

Table 1. Quadrotor Parameters Specification

Parameter	Description	Value/Unit
m	Quadrotor mass	1.79 kg
$\boldsymbol{\ell}$	Motor to c.g. distance	0.18 m.
$\boldsymbol{I}$	Moment of inertia matrix	1.335×10^{-2} [1, 1, 1.85] kg.m^2
g	Gravity acceleration	9.81 m/sec^2

$\mathbf{k}_f$	Thrust coefficient	8.82×10^{-6} N/(rad/sec)^2
$\mathbf{k}_m$	Drag coefficient	1.09×10^{-7} N.m/(rad/sec)^2
$\boldsymbol{e_0(x,y,z)}$	Initial position error	[2, -2, 0] m.
$\boldsymbol{\phi_0, \theta_0, \psi_0}$	Initial Euler angles	[0, 0, 0]. rad
$\boldsymbol{\mathcal{A}}$	Disturbance amplitudes	[3,3,3].
$\boldsymbol{w}$	Disturbance frequency	5 rad/sec

For the purpose of the simulation study, the vectors that represent the impact of uncertainty and disturbance in Eq. (11) and Eq. (12) are assumed to be time-varying harmonic signals as follows,

$$\Delta_{1,2}(\mathrm{t}) = \mathcal{A}\sin(w\ \mathrm{t}), \tag{30}$$

where, $\mathcal{A} \in \mathbb{R}^3$ is a vector representing the disturbance amplitudes, w is the disturbance frequency. The desired trajectory of quadrotor robot has been chosen to be a trajectory that passes sequentially through predefined nine waypoints and at the same time achieving the specified yaw angles at each waypoint. Furthermore, the waypoints' timing can also be prespecified or optimized based on the segments lengths and turning angles. The path connecting the waypoints is designed such that, the second derivative of acceleration "snap" is minimum along the entire segments. The desired mission profile is shown in Fig. 4. The waypoints coordinates and instantaneous heading angles are described as follows,

$$r_1 = [-5, 0, 0\ ]m\ , r_2 = [10, -5, 15]m, r_3 = [25, 15\ , 20]m\ , r_4 = [15\ , 20, 30]m\ ,$$
$$r_5 = [5, 5\ , 30]m\ , r_6 = [15, -5, 30]m\ , r_7 = [25, 5\ , 30]m\ , \quad r_8 = r_4\ , \quad r_9 = r_1\ ,$$
$$\psi_{1\_to\_9} = [0^0\ , 30^0, 60^0\ , 90^0\ , 90^0\ , 90^0\ , 90^0\ , 90^0\ , 180^0].$$

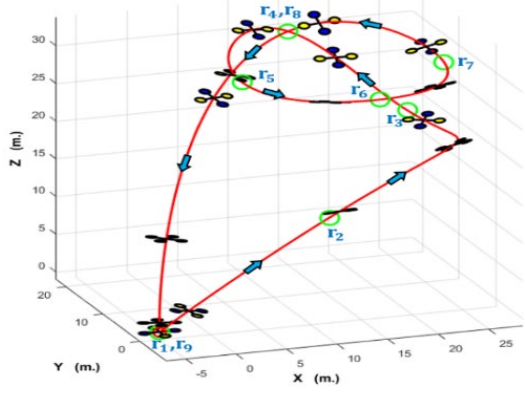

Fig. 4 The 3D Trajectory of the Desired Mission Profile

The mission configuration is to take off from r_1. Then to climb to r_4 through r_2 and r_3. After that, to conduct a circular-like maneuver through r_5, r_6, r_7 and r_8. Finally, to return to land at the same take-off point. The mission completion time is predefined to be 25 sec. The controllable parameters of each controller are tuned using our developed search algorithm based on the genetic algorithm such that, the integral time of absolute error (ITAE) is minimum and the required rotor speeds are within the design limits.

5.1 Simulation without Parameters Uncertainty and Disturbance Sources

The simulation is performed for the mentioned four control schemes to evaluate the efficiency of each control algorithm in steering quadrotor robots to follow a certain desired trajectory based on the nonlinear model illustrated in Eq. (1) and Eq. (4). The desired mission has been

chosen such that, the initial position error is relatively large, $|e_0| = 2.83\ m$, and the trajectory is highly manoeuvrable with strict boundary and intermediate conditions in order to arrive at a near-real assessment of the different control approaches. The 3D desired trajectory and actual dynamical trajectories of each controller are shown in Fig. 5.

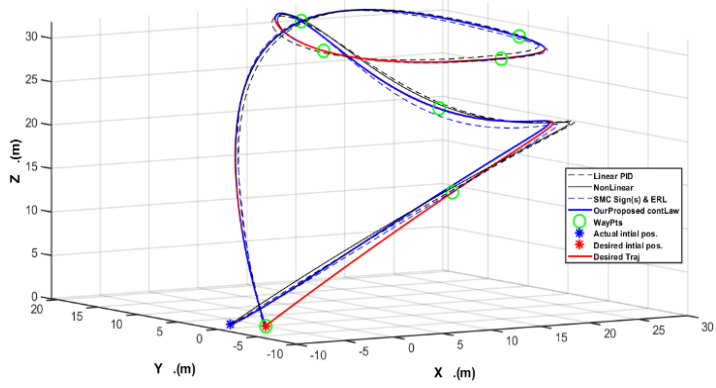

Fig. 5 3D-Trajectory Tracking Performance of the Four Control Schemes, Case (i)

The time history of the robot six state variables, $[x\ ,y\ ,z, \phi\ ,\theta\ ,\psi]$ are shown in Fig. 6 and Fig. 7 respectively. The three components of linear velocities, $[\ \dot{x}\ ,\dot{y}\ ,\dot{z}\ ]$ as well as the angular velocities, $[\ p\ ,\ q,\ r]$ are demonstrated in Fig. 8 and Fig. 9, respectively. To clearly illustrate the main differences in the performance indicators of each control approach, the qualitative analysis also demonstrates the trajectory error history and the necessary rotor speeds, Ω_i^{des} that obtained using the transformation matrix, Eq. (7) as shown in Fig. 10 and Fig. 11, respectively. It can be observed from Fig. 10 that, using a linear PID controller with a nonlinear model of quadrotor may lead to a relatively high tracking error, especially at the segments required high turning angles.

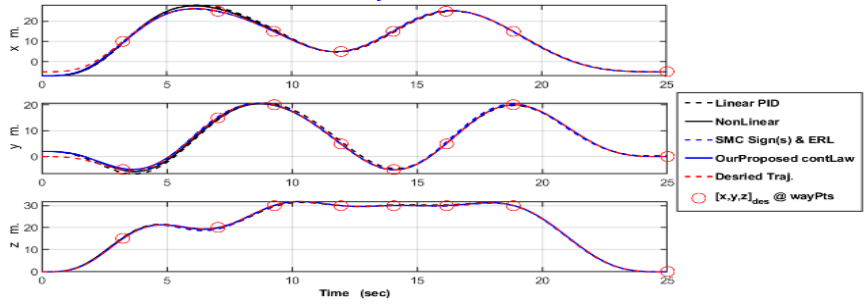

Fig. 6 Comparison of Positions Variation, Case (i)

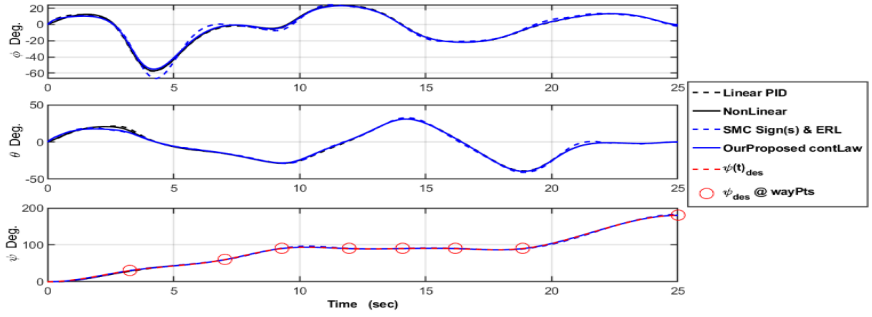

Fig. 7 Comparison of Euler-Angles Variation, Case (i)

Although the conventional SMC with ERL produces good tracking performance, the chattering effect clearly appears at the angular velocities and rotor speeds as shown in Fig. 9 and Fig. 11, respectively. The nonlinear GTC provides satisfactory tracking error and the norm of the error reaches zero after 12.5 seconds. However, our robust hybrid control law achieved better tracking error, and according to the simulation settings, the error magnitude exponentially converges to zero after about 6.5 seconds.

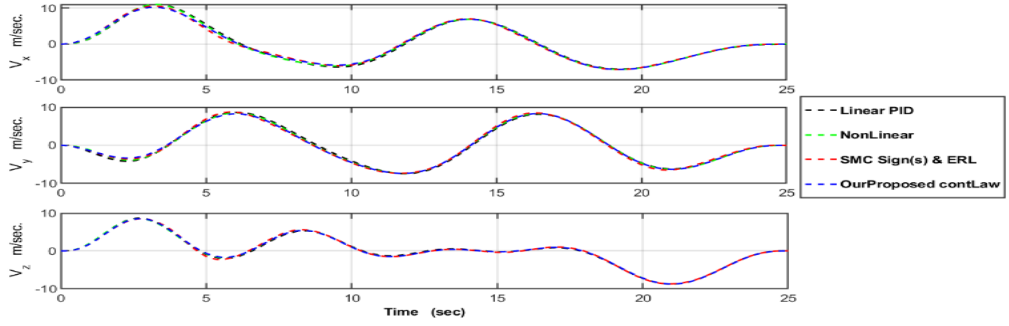

Fig. 8 Comparison of Velocities Variation, Case (i)

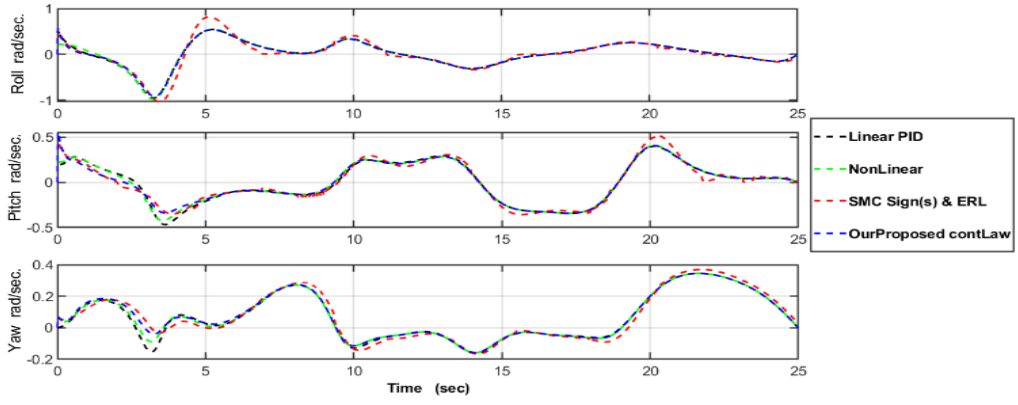

Fig. 9 Comparison of Angular-Velocities Variation, Case (i)

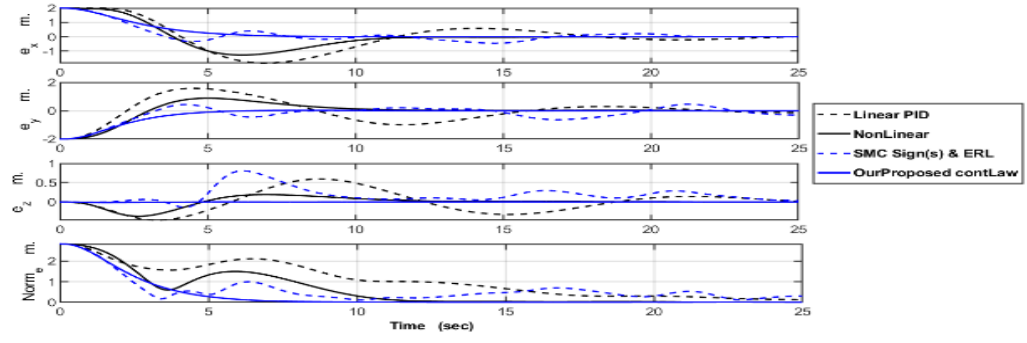

Fig. 10 Comparison of Positions Error Variation, Case (i)

5.2 Simulations with Uncertain Disturbances for Position and Orientation States

In this subsection, the nonlinear uncertain dynamics model illustrated in Eq. (11) and Eq. (12) are adopted. The bounds of uncertain disturbances selected to be relatively large, $|\Delta(t)| \leq$ 3m, and affecting all robot states. The 3D trajectories of the four proposed control laws and the mission desired trajectory are shown in Fig. 12.

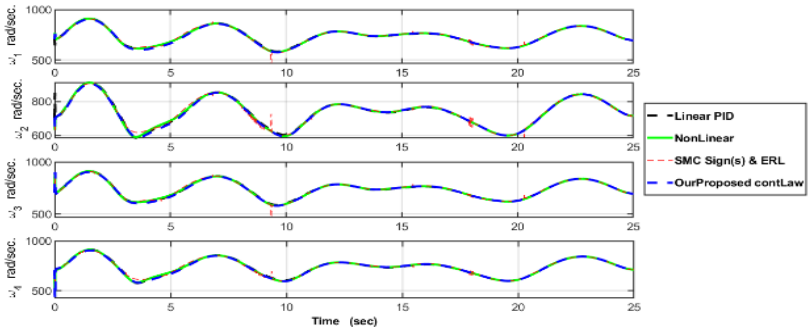

Fig. 11 Comparison of Desired Rotor-Speeds Variation, Case (i)

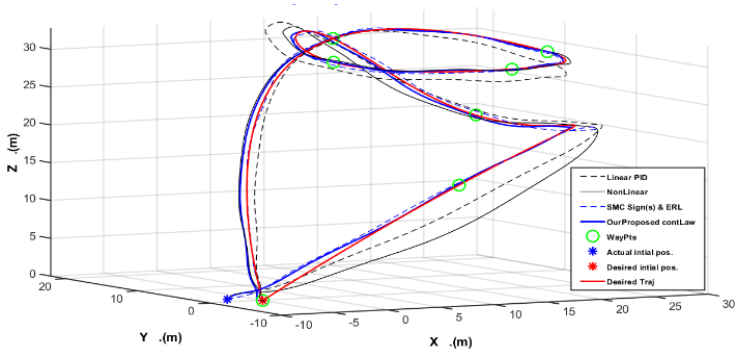

Fig. 12 3D-Trajectory Tracking Performance of the Four Control Schemes, Case (ii)

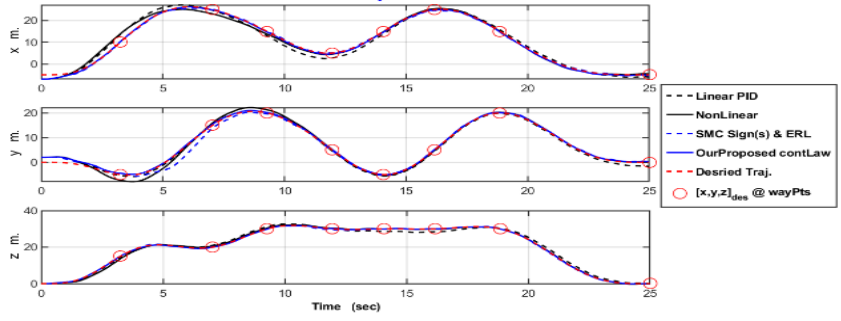

Fig. 13 Comparison of positions Variation, Case (ii)

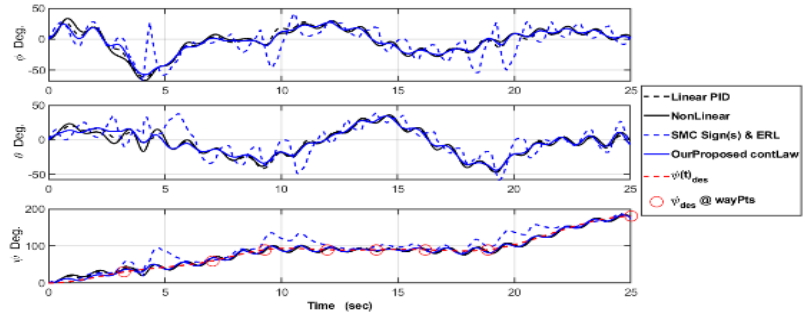

Fig. 14 Comparison of Euler-Angles Variation, Case (ii)

Obviously, the terms representing the uncertainties and disturbances have a significant impact on the overall performance to varying degrees. In Fig. 13 and Fig. 14, the quadrotor position and attitude states are demonstrated, respectively. The robot linear and angular velocities are shown in Fig. 15 and Fig. 16, respectively.

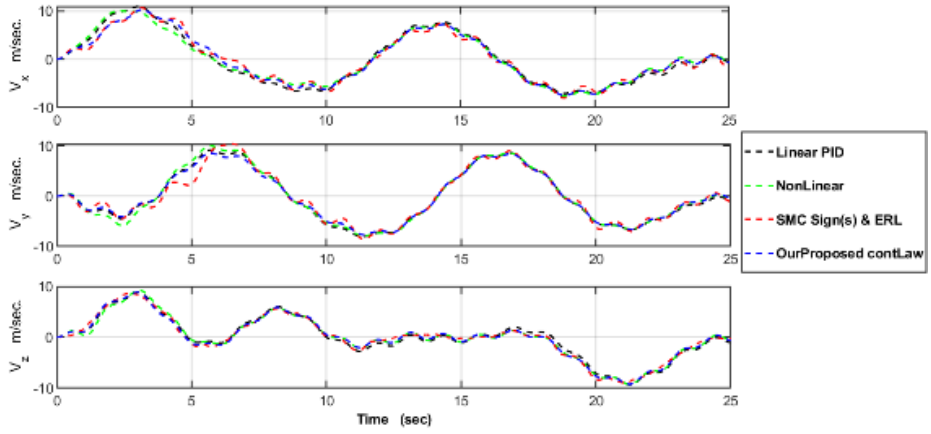

Fig. 15 Comparison of velocities Variation, Case (ii)

Results observations illustrated in Fig. 17 show that the PID controller is no longer a good choice to be applied to such settings as it produces a relatively large tracking error, more than 1.5 meters about the desired trajectory. The conventional SMC has better tracking error by exploiting the features of ERL, however, the required rotor speeds fall outside the design range, and the switching signum function leads to relatively high oscillation in the attitude control as shown in Fig. 14. On the other hand, the simulation results demonstrated that, even with the considerable impact of the uncertainties and disturbances, our proposed hybrid control laws also provide better tracking performance with a steady-state error of less than 6.6% of $\mathcal{A}$, and robustly achieving asymptotic stability within the design range of rotor speeds.

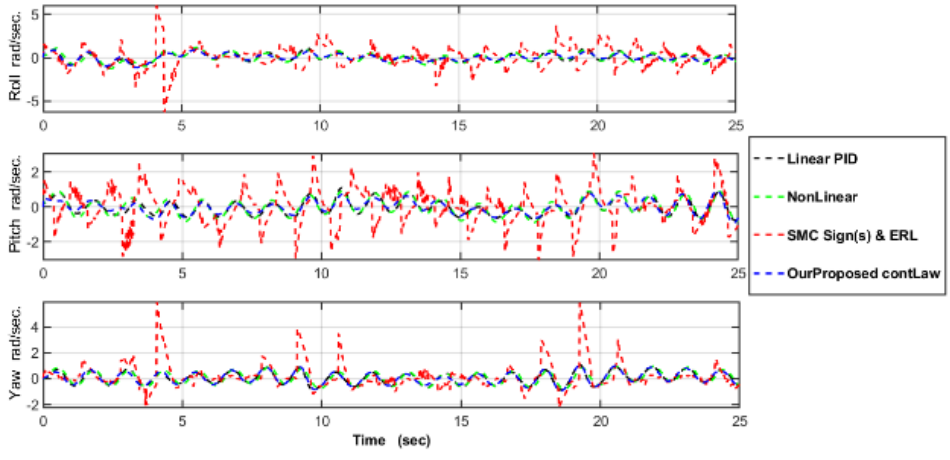

Fig. 16 Comparison of Angular-Velocities Variation, Case (ii)

The simulation results also reflected the utility aspects underlying the control concepts included in the proposed hybrid control law. Whereas, NFC with GTC improved the attitude control performance and ERL enhanced the tracking error. Furthermore, the SMC that uses a saturation function with time-varying parameter $\varphi(t)$, dealt with the parameter uncertainties, achieved robust stability, treated the chattering phenomenon, provided optimal time control, and tackled the sensitivity dilemma of NFC. Due to page limit constrain, supplementary material of this work is available in [(1)], to simulate more animated scenarios and present more features of our proposed hybrid control approaches.

[(1)] https://www.youtube.com/watch?v=Id04qiFTu-c

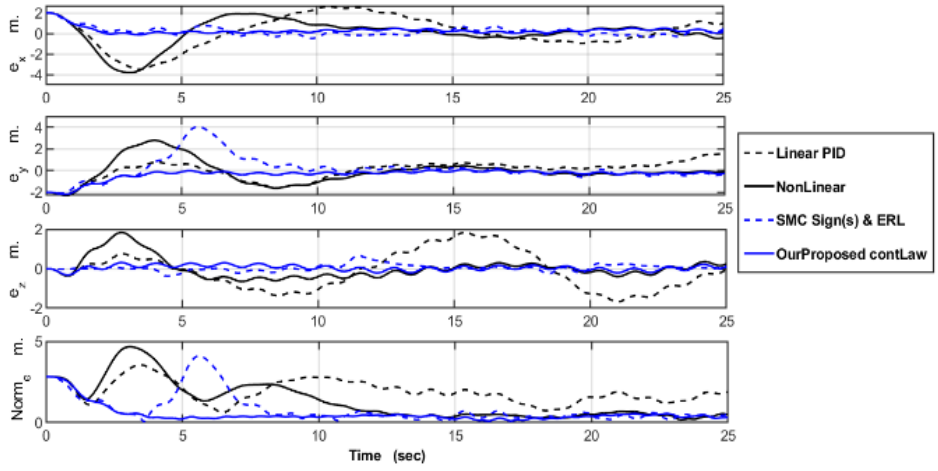

Fig. 17 Comparison of positions Error Variation, Case (ii)

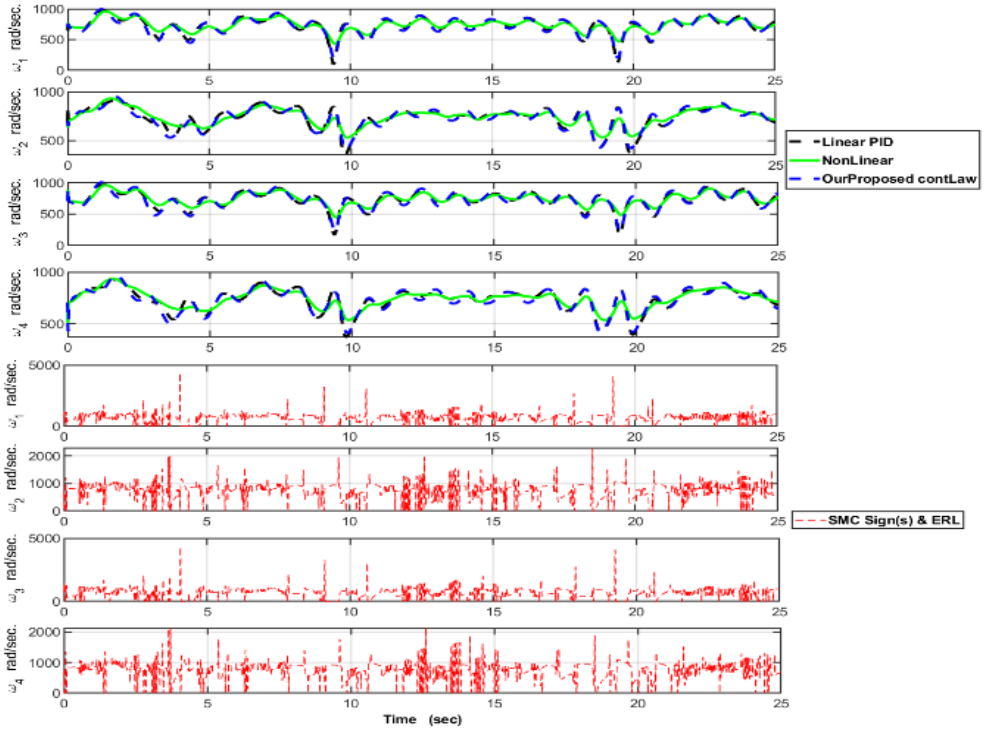

Fig. 18 Comparison of Desired rotor-speeds variation, Case (ii)

6. CONCLUSIONS

This research paper proposed a novel robust hybrid SMC with GTC and NFC, to efficiently address the trajectory tracking problems of aerial robots. The compound control schemes have been derived and developed based on the nonlinear dynamic model of quadrotors robot, taking into account the model uncertainties as well as the considerable disturbances that may affect the system performance. Furthermore, the proposed control algorithms exploited the advantages of GTC, ERL, NFC, and SMC with an adjustable saturation function, to overcome the chattering uncertainty effect and arrived at enhanced trajectory tracking performance

regardless of the external disturbance sources. The QCA along with MATLAB 3D simulation results demonstrated the robustness, asymptotic stability, and applicability of the proposed controllers in real agile autonomous flying robots to accurately achieve complex trajectory-tracking missions.

7. APPENDIX

A.1 Preliminaries and Notions of SMC

The mathematical dynamic model of the aerial robot may experience model inaccuracies in either of the following two forms: (i) structural uncertainties due to parameters imprecision or (ii) unmodeled dynamics resulting from simplifying the model dynamics such as ignoring the non-dominant dynamics. Furthermore, in reality, the system dynamics are almost subjected to external disturbances. The modeling uncertainty dilemma usually dealt with by adopting one of the popular two approaches, (i) employing a time-variant controller to control time-invariant system, namely, an adaptive control approach, or (ii) using a time-invariant controller to deal with a time-variant system which is commonly known as robust control approach such as SMC. The main idea behind the SMC is that, instead of directly dealing with nth order system to be controlled, we attempt to define a new intermediate variable S "sliding surface" with 1st order dynamics, i.e. the equation that relates the variable, S to the system input, u is a first-order differential equation. Therefore, the SMC is known as a time-optimal control [20]. In other words, since the relation between S and u is a first order dynamics, the control action is either positive to increase the output or negative to decrease it. The demerit of such a controller property is that, the control action is discontinuous at the sliding surface and thus around the desired trajectory leading to the chattering phenomenon [21].

A.2 The Problem Formulation of SMC

The conventional SMC is considered as a nonlinear control algorithm that employs a switching or discontinuous control signal to command the system to slide along a prespecified surface without any simplification for system dynamics. Consider the nth order dynamic system,

$$x^{(n)} = f\left(t, x, \dot{x}, \dots, x^{(n-1)}\right) + g(t, x, \dot{x}, \dots)\, u + \Delta(t) \tag{31}$$

where, $x \in \mathbb{R}^m$ is the state vector of m states, $f(*)$ and $g(*)$ are differentiable and uncertain nonlinear functions, u is the control vector. The vector $\Delta(t)$ represents the parameter uncertainties and/or the external disturbances, such that, $\Delta_L \leq \Delta(t) \leq \Delta_U$, where, Δ_U and Δ_L are known upper and lower bounds of the uncertain disturbances.

A.3 Design Procedures of SMC

The two major steps during the SMC design procedure are, (i) Determine the sliding surface such that, $\dot{S}$ contains the system input u, and S tends to zero as the tracking error approaches zero, and (ii) Define the control signal u as two terms, the first term is nonlinear feedback to cancel the known terms and thus drives $\dot{S}$ of the known system to zero. The second term, to compensate for uncertainty and achieve Lyapunov stability and thus satisfy the sliding condition. For nth order system, the sliding surface is defined as

$$S = e(t)^{(n-1)} + C_1\, e(t)^{(n-2)} + C_2\, e(t)^{(n-3)} + \cdots + C_{n-1}\, e(t) \tag{32}$$

where, $e(t)$ is the tracking error, $e(t) = x_{des}(t) - x(t)$.

The sliding condition for the classical SMC is, $S\,\dot{S} \leq 0$.

However, to control the approaching time and velocity to the sliding surface, the sliding condition is modified to, $S\,\dot{S} \leq \delta(t)$, such that, $\delta(t) \leq 0$. For conventional SMC, $\delta(t)$ is chosen to be,

$$\delta(t) = -\,\eta\, S\, sign\,(S), \quad \eta > 0 \tag{33}$$

REFERENCES

[1] Y. Xu, Y. S. Shmaliy, X. Chen, Y. Li, and W. Ma, Robust inertial navigation system/ultra wide band integrated indoor quadrotor localization employing adaptive interacting multiple model-unbiased finite impulse response/Kalman filter estimator, *Aerosp. Sci. Technol.*, vol. **98**, p. 105683, 2020, doi: 10.1016/j.ast.2020.105683.

[2] G. M. Qian, D. Pebrianti, Y. W. Chun, Y. H. Hao, and L. Bayuaji, Waypoint navigation of quad-rotor MAV, in *2017 7th IEEE International Conference on System Engineering and Technology (ICSET)*, pp. 38–42, 2017.

[3] D. Xilun, G. U. O. Pin, X. U. Kun, and Y. U. Yushu, A review of aerial manipulation of small-scale rotorcraft unmanned robotic systems, *Chinese J. Aeronaut.*, vol. **32**, no. 1, pp. 200–214, 2019.

[4] M. Bernard and K. Kondak, Generic slung load transportation system using small size helicopters, in 2009 *IEEE International Conference on Robotics and Automation*, pp. 3258–3264, 2009.

[5] S. Berrahal, J. H. Kim, S. Rekhis, N. Boudriga, D. Wilkins, and J. Acevedo, Border surveillance monitoring using Quadcopter UAV-Aided Wireless Sensor Networks, *J. Commun. Softw. Syst.*, vol. **12**, no. 1, pp. 67–82, 2016, doi: 10.24138/jcomss.v12i1.92.

[6] Q. Zhan, J. Wang, and X. Xi, Control system design and experiments of a quadrotor, in *2012 IEEE International Conference on Robotics and Biomimetics (ROBIO)*, pp. 1152–1157, 2012.

[7] S. Bouabdallah, A. Noth, and R. Siegwart, PID vs LQ control techniques applied to an indoor micro quadrotor, in *2004 IEEE/RSJ International Conference on Intelligent Robots and Systems (IROS)(IEEE Cat. No. 04CH37566)*, vol. **3**, pp. 2451–2456, 2004.

[8] P. S. G. Cisneros, C. Hoffmann, M. Bartels, and H. Werner, Linear parameter-varying controller design for a nonlinear quad-rotor helicopter model for high speed trajectory tracking, in *2016 American Control Conference (ACC)*, pp. 486–491, 2016.

[9] M. Sun and J. Liu, Tracking control of a quad-rotor UAV based on T—S fuzzy model, in *2017 36th Chinese Control Conference (CCC)*, pp. 4216–4221, 2017.

[10] C.-L. Hwang, Hybrid neural network under-actuated sliding-mode control for trajectory tracking of quad-rotor unmanned aerial vehicle, in *The 2012 International Joint Conference on Neural Networks (IJCNN)*, pp. 1–8, 2012.

[11] L. Wang, C. He, and P. Zhu, Adaptive sliding mode control for quadrotor aerial robot with I type configuration, *Int. J. Autom. Control Eng.*, vol. **3**, pp. 20–26, 2014.

[12] R. Kumar, M. Dechering, A. Pai, A. Ottaway, M. Radmanesh, and M. Kumar, Differential flatness based hybrid PID/LQR flight controller for complex trajectory tracking in quadcopter UAVs, *Proc. IEEE Natl. Aerosp. Electron. Conf. NAECON*, vol. *2017-June*, pp. 113–118, doi: 10.1109/NAECON.2017.8268755, 2017.

[13] T. Lee, M. Leok, and N. H. McClamroch, Geometric tracking control of a quadrotor UAV on SE (3), in *49th IEEE conference on decision and control (CDC)*, pp. 5420–5425, 2010.

[14] R. Hamrah and A. K. Sanyal, Finite-time stable tracking control for an underactuated system in SE(3) in discrete time, *Int. J. Control*, pp. 1–16, doi: 10.1080/00207179.2020.1841299, Nov. 2020.

[15] J. Zhang, D. Gu, Z. Ren, and B. Wen, Robust trajectory tracking controller for quadrotor helicopter based on a novel composite control scheme, *Aerosp. Sci. Technol.*, vol. **85**, pp. 199–215, 2019.

[16] Z. Shen, F. Li, X. Cao, and C. Guo, Prescribed performance dynamic surface control for trajectory tracking of quadrotor UAV with uncertainties and input constraints, *Int. J. Control*, pp. 1–11, Mar. 2020, doi: 10.1080/00207179.2020.1743366.

[17] K. Alexis, G. Nikolakopoulos, and A. Tzes, Model predictive quadrotor control: attitude, altitude and position experimental studies, *IET Control Theory Appl.*, vol. **6**, no. 12, pp. 1812–1827, 2012.

[18] K. Runcharoon and V. Srichatrapimuk, Sliding mode control of quadrotor, in *2013 The International Conference on Technological Advances in Electrical, Electronics and Computer Engineering (TAEECE)*, pp. 552–557, 2013.

[19] H. Ríos, R. Falcón, O. A. González, and A. Dzul, Continuous sliding-mode control strategies for quadrotor robust tracking: real-time application, *IEEE Trans. Ind. Electron.*, vol. **66**, no. 2, pp. 1264–1272, 2018.

[20] R. Dong and G. Y. Tang, Optimal sliding mode control for linear systems with time-delay, *Conf. Proc. - IEEE Int. Conf. Syst. Man Cybern.*, vol. **6**, no. 1, pp. 4524–4528, doi: 10.1109/ICSMC.2006.384858, 2006.

[21] R. Niemiec and F. Gandhi, A comparison between quadrotor flight configurations, *42nd Eur. Rotorcr. Forum 2016*, vol. *1*, pp. 186–197, 2016.

[22] C. Wang, Z. Chen, and M. Sun, Sliding mode control of a quadrotor helicopter, *Zhongnan Daxue Xuebao (Ziran Kexue Ban)/Journal Cent. South Univ.* (*Science Technol.*, vol. **48**, no. 4, pp. 1006–1011, doi: 10.11817/j.issn.1672-7207.2017.04.021, 2017.

[23] N. Ahmed and M. Chen, Sliding mode control for quadrotor with disturbance observer, *Adv. Mech. Eng.*, vol. **10**, no. 7, pp. 1–16, doi: 10.1177/1687814018782330, 2018.

[24] R. Kumar, M. Dechering, A. Pai, A. Ottaway, M. Radmanesh, and M. Kumar, Differential flatness based hybrid pid/lqr flight controller for complex trajectory tracking in quadcopter uavs, in *2017 IEEE National Aerospace and Electronics Conference (NAECON)*, pp. 113–118, 2017.

[25] D. W. Mellinger, *Trajectory generation and control for quadrotors*, 2012.

[26] C. J. Fallaha, M. Saad, H. Y. Kanaan, and K. Al-Haddad, Sliding-mode robot control with exponential reaching law, *IEEE Trans. Ind. Electron.*, vol. **58**, no. 2, pp. 600–610, 2010.

[27] W. Gao and J. C. Hung, Variable Structure Control of Nonlinear Systems: A New Approach, *IEEE Trans. Ind. Electron.*, vol. **40**, no. 1, pp. 45–55, doi: 10.1109/41.184820, 1993.

[28] M. El Naggar, *Nonlinear Control 2 Sliding Mode Control*, 2020, Cairo University. https://www.youtube.com/watch?v=qMoP9EJgQrA (accessed Sep. 29, 2020).